Optimization of SAR Distributions in Liver and Lung Regions Irradiated by the *H*-Horn Annular Phased Array Hyperthermia System

Tianquan Deng

Abstract—**This paper discusses a new type of annular phased array system—the *H*-horn APA. The phase and amplitude control of power deposition patterns for this system has been theoretically analyzed at a frequency of 200 MHz. The formulas for calculating the *E* field and SAR for this APA system have been derived, and can be applied to other types of APA systems. Models on computerized tomography (CT) scans from liver and lung regions have been used for predicting optimization of the *E* field and SAR patterns in the case of the relative phase and amplitude changes. It is shown that the technique of the phase and amplitude control of SAR patterns results in a more selective and effective heating of tumors situated eccentrically and deeply within the body. The APA hyperthermia system described in this paper shows great promise, and looks very useful for developing clinical applications.**

I. Introduction

ONE of the greatest technical challenges so far faced by hyperthermia researchers has been the development of a means of selectively heating deep-seated tumors. Previous reports [1] indicate that it is possible to focus electromagnetic power directly into the deepest regions to treat a variety of human tumors. The development which achieves therapeutic heating in deep tumors while sparing normal surface tissues is the annular phased array (APA). This local noninvasive electromagnetic hyperthermia technique shows great promise for clinical applications. Most applicators used for APA have taken the form of apertures or waveguides [1]–[5]. And several papers (e.g. [3], [6], and [7]) have been published concerning optimization methods to determine the phases and amplitudes in treating deep-seated tumors with APA systems, including three-dimensional cases [8], [9].

This paper considers the use of *H*-horn antennas as applicators, and adopts a frequency of 200 MHz, which is suitable for the deep regions of the abdomen and chest. Attention is also given to *H*-horn antennas with deionized distilled water loading.

Manuscript received July 10, 1990; revised November 19, 1990.

The author is with the Research Institute of High Energy and Microwave Electronics, University of Electronic Science and Technology of China, Chengdu 610054, People's Republic of China.

IEEE Log Number 9142998.

A new type of annular phased array system is described in this paper, one where each radiating element of the APA system is an *H*-horn antenna. Formulas for calculating the *E* field and specific absorption rate (SAR) for this APA system have been obtained. The phase and amplitude control of power deposition patterns for this APA system has been theoretically analyzed at a frequency of 200 MHz. First, the *E* field distributions of circular cylindrical dielectric shells and circular cross sectional cylindrical dielectric structures have been studied and are compared with published results. Then models of computerized tomography scans from the liver and lung regions have been treated for predicting the optimization of *E* and SAR patterns by varying the phase and amplitude of the horn antenna's radiation. In principle, the formulas and numerical methods described in this paper can be applied to other types of APA systems. The numerical results indicate that it is possible to shift the absorbed power patterns by electrically varying the phase and/or the amplitude of the sources and manually moving the positions of the horns.

II. APA System

The APA, shown in Fig. 1, consists of six radiating *H*-horn antennas arranged in annular form (more or less, even multilayer antennas are acceptable). The patient is placed inside the central opening of the antenna array with deionized distilled water boluses filling the horns and the spaces between the patient and the antenna surfaces. This can improve the energy coupling from the bolus to the body, reduce the size of the antenna, and provide a surface temperature control to obtain uniform heating with the distilled water for cooling. The power losses in the water are negligible because of the low conductivity of the deionized water. The *H*-horn applicator has its own characteristics, which include a low level of environmental pollution, good impedance matching between the body and the horns, and easy motion of the horns to adjust the array elements independently.

For simplicity, the system is assumed to be a two-dimensional configuration in which all the parameters

0018-9480/91/0500-0852$01.00

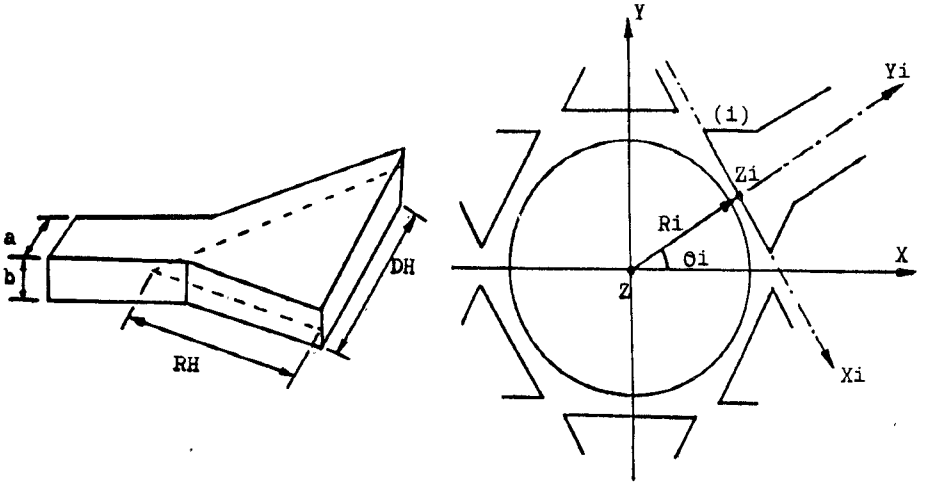

Fig. 1. APA system and its coordinate system. *DH* and *RH* give the size of the horn, and (R_i, θ_i) is the position of antenna i.

vary only in the $X-Y$ plane and the electric field is polarized along the Z axis.

In practice, in order to control the phase and amplitude electrically, a coherent phase and amplitude difference can be created by varying the length of the input cable, using high-power variable attenuators, or adopting a multichannel amplifier to be controlled by a microcomputer.

III. Theoretical Background

The moment methods and the microwave scattering theory used in this paper have been described in [10] and [11]. It has been shown (for an $\exp(j\omega t)$ time dependence) that the integral equation relating the total electric field (E) at any point (X,Y) inside the body is given by

$$E(X,Y)+jK_0^2/4\int_{\text{sec.}}\int(\epsilon-1)E(X',Y')\cdot H_0^{(2)}(K_0\rho)\,dX'\,dY'=E^{\text{I}}(X,Y) \quad (1)$$

where $K_0=2\pi/\lambda_0$, $H_0^{(2)}(K_0\rho)$ is the zero-order Hankel function of the second kind, and ρ is given by

$$\rho=\sqrt{(X-X')^2+(Y-Y')^2}. \quad (2)$$

$E^{\text{I}}(X,Y)$ is the total incident field from the APA sources:

$$E^{\text{I}}(X,Y)=\sum_{i=1}^{6}E_i=\sum_{\iota=1}^{6}(C_\iota+jD_\iota) \quad (3)$$

where E_ι is the incident field from each of the six sources polarized in the Z direction.

In Fig. 1, in the $X_\iota Y_\iota Z_\iota$ coordinate system, E_ι is given by

$$E_\iota(X_\iota,Y_\iota)=A_\iota\int_{-DH/2}^{DH/2}E_{zi}(X_0,0)\frac{\partial}{\partial n}H_0^{(2)}\cdot\left\{K_0\left[(X_i-X_0)^2+Y_\iota^2\right]^{1/2}\right\}dX_0 \quad (4)$$

where X_0 is the distance along the X_i axis, and $E_{zi}(X_0,0)$ is the field distribution on the edge plane of each source:

$$E_{zi}(X_0,0)=E_{0i}\cos(\pi X_0/DH)\cdot\exp\left[-j\pi X_0^2/(\lambda RH)\right]\exp(-j\phi_\iota). \quad (5)$$

Here ϕ_ι is the required phase shift, *DH* and *RH* give the size of the horn (shown in Fig. 1; typical designed parameters: $DH=23$ cm and $RH=22$ cm according to antenna theory).

And if we let

$$\exp\left(-j\pi X_0^2/\lambda RH\right)=1 \quad (6)$$

we can get the same form as described in [3] and [4]. In the XYZ coordinate system, C_ι and D_ι will be given by

$$C_\iota=A_\iota\int_{-DH/2}^{DH/2}\left[X\cos(\theta_\iota)+Y\sin(\theta_\iota)-R_\iota\right]/\rho*\cos(\pi X_\iota/DH)\left[J_1(K_0\rho)\sin\left(\pi X_\iota^2/\lambda RH+\phi_\iota\right)+Y_1(K_0\rho)\cos\left(\pi X_\iota^2/\lambda RH+\phi_\iota\right)\right]dX_\iota \quad (7)$$

$$D_\iota=A_\iota\int_{-DH/2}^{DH/2}\left[X\cos(\theta_\iota)+Y\sin(\theta_\iota)-R_\iota\right]/\rho*\cos(\pi X_\iota/DH)\left[J_1(K_0\rho)\cos\left(\pi X_\iota^2/\lambda RH+\phi_\iota\right)-Y_1(K_0\rho)\sin\left(\pi X_\iota^2/\lambda RH+\phi_\iota\right)\right]dX_\iota \quad (8)$$

where $H_1^{(2)}(x)=J_1(x)-jY_1(x)$ is the first-order Hankel function of the second kind and ρ is given by

$$\rho=\left\{\left[X\sin(\theta_i)-Y\cos(\theta_\iota)-X_\iota\right]^2+\left[X\cos(\theta_i)+Y\sin(\theta_i)-R_\iota\right]^2\right\}^{1/2}. \quad (9)$$

$E_i=C_\iota+jD_\iota$ and (R_i,θ_i) is the position of antenna i.

Equation (1) can be solved numerically using the moment methods [10] by dividing the cross section into N small cells and assuming the field and complex permittivity to be constant in each cell:

$$E_m+jK_0^2/4\sum_{n=1}^{N}(\epsilon_n-1)E_n\int_{\text{cell}}\int_n H_0^{(2)}\cdot(K_0\rho_{mn})\,dX_n\,dY_n=E_m^{\text{I}}\qquad(m=1,\cdots,N) \quad (10)$$

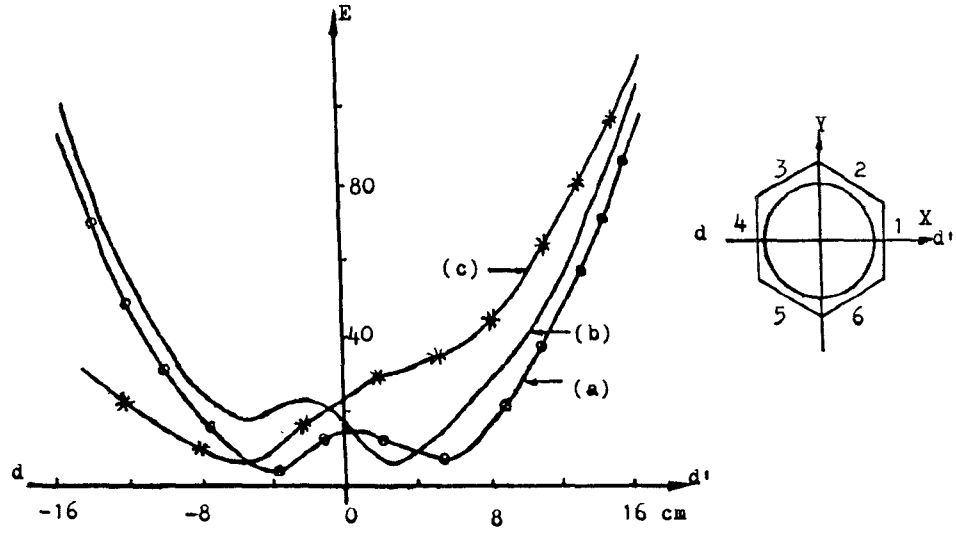

Fig. 2. Numerical results for the cylindrical model: (*a*) Equal phase and amplitude on all antennas; (*b*) Equal amplitude, 90° phase lag on antennas 3, 4, and 5; (*c*) 90° phase lag and 30% amplitude reduction on antennas 3, 4, and 5.

where ϵ_n and E_n are the complex permittivity and the unknown total electric field in cell n, respectively. Using the concept of equivalent circular cell [11], (10) can be integrated in closed form. Hence,

$$\sum_{n=1}^{N} G_{mn}E_{mn} = E_m^I \qquad (m=1,2,\cdots,N) \qquad (11)$$

where

$$G_{mn} = 1+0.5j(\epsilon_n-1)\left[\pi K_0 a_n H_1^{(2)}(K_0 a_n) - 2j\right] \qquad (m=n) \quad (12)$$

$$G_{mn} = (0.5j\pi K_0 a_n)(\epsilon_n-1)J_1(K_0 a_n)H_0^{(2)}(K_0\rho_{mn}) \qquad (m\neq n). \quad (13)$$

Then the absorbed power density or SAR in the tissues for each cell is given by

$$\text{SAR} = \frac{1}{2}\sigma|E|^2/\rho \text{ (W/kg)} = \pi f\epsilon_0\epsilon''|E|^2/\rho \text{ (W/kg)} \qquad (14)$$

where σ is the conductivity (S/m), ρ is the density (kg/m^3), ϵ'' is the loss factor of tissue in the cell, and f is the operating frequency.

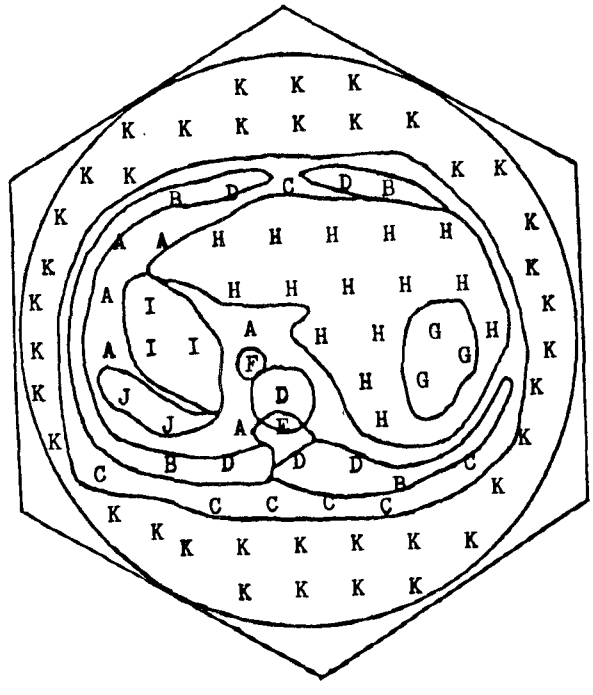

Fig. 3. Liver model: The actual size of the section $33*28$ cm^2.

IV. Numerical Results and Discussion

A. The Cylindrical Shell and Cylindrical Structure Models

First, the electric field distributions inside a circular cylindrical dielectric shell with incident plane waves have been calculated. It is found that these numerical results agree very well with the exact solutions described in Richmond's paper [11]. Then a circular cylindrical structure placed centrally in the APA has been studied. The homogeneous model also provides a good check on the validity of this numerical method. The cylinder has a diameter of 32 cm and consists of a musclelike medium which has a real permittivity $\epsilon' = 56.0$, an imaginary permittivity $\epsilon'' = 90.0$, a conductivity $\sigma = 1.0$ s/m, and a density $\rho = 1.02*10^3$ kg/m^3 at 200 MHz. The cross-sectional area is divided into 224 cells.

The E-field distributions along the diammeter dd' are shown in Fig. 2. It is clear that the central maximum point of the electric field shifts significantly with changes in the phase and amplitude of the horns.

B. Liver Model and Lung Model

Models of the liver with 329 cells and of the lung with 158 cells are shown in Figs. 3 and 4 respectively. The cell centers are denoted by the respective tissues they represent. The properties of these tissues are given in Table I [12].

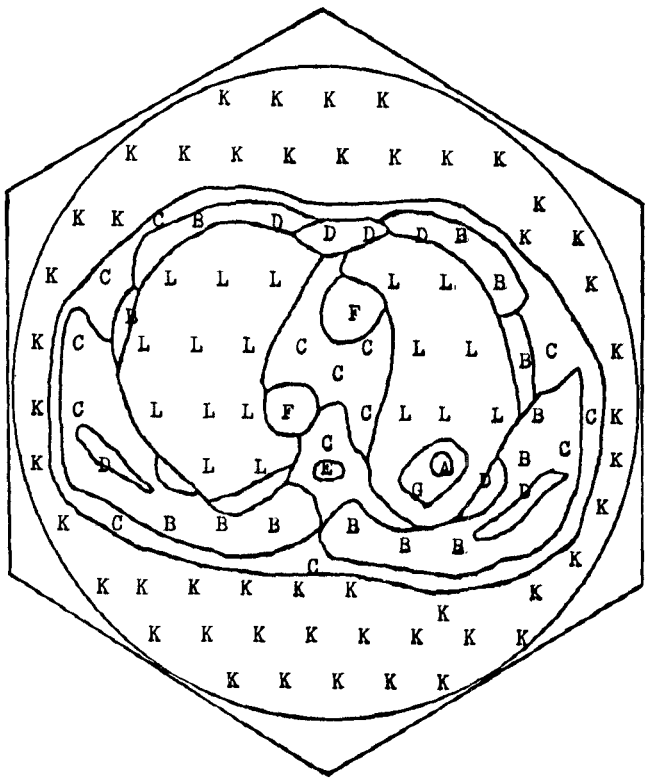

Fig. 4. Lung model: The actual size of the section is $31 * 27$ cm^2.

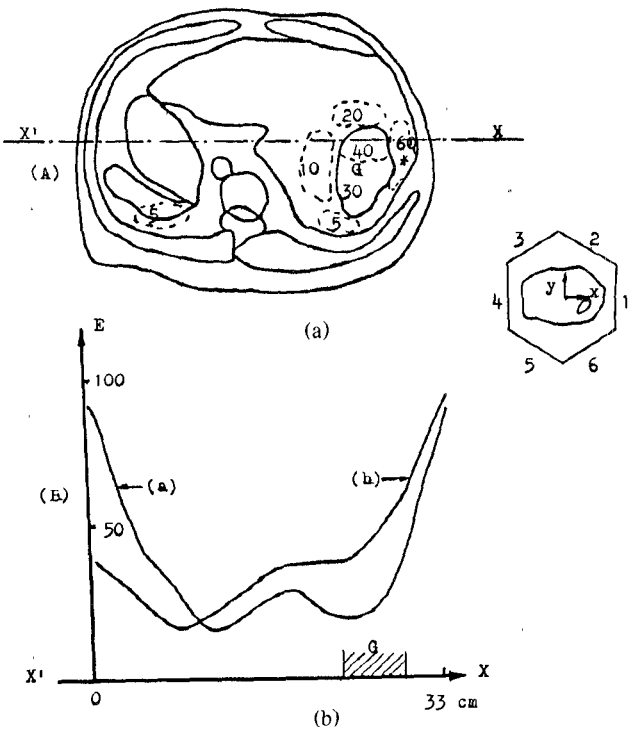

Fig. 5. Numerical results of the liver model. (a) Optimized SAR contours in the liver region (the phase and amplitude conditions are the same as those given in part (b), curve (*b*) of this figure). (b) *E*-field distributions along *XX'*. Curve (*a*) represents equal phase and amplitude on all antennas; curve (*b*) represents 150° phase lag and 25% amplitude reduction on antennas 3, 4, and 5 and 50% amplitude reduction on antennas 2 and 6.

TABLE I
PROPERTIES OF TISSUES IN THE LIVER AND LUNG MODELS AT 200 MHz

Tissue	ϵ'	ϵ''	$\rho * 10^3$ kg/m^3
A air	1.0	0.0	
B muscle	56.0	90.0	1.02
C fat	5.6	3.7	0.9
D bone	5.6	3.7	1.79
E spinal cord	5.0	2.5	1.0
F blood	63.0	90.0	1.0
G tumor	56.0	90.0	1.02
H liver	50.0	70.0	1.02
I stomach	56.0	90.0	1.02
J spleen	56.0	90.0	1.02
K distilled water	76.0	0.0	1.0
L lung	35.0	56.0	1.02

C. Discussion

The numerical results, shown in Figs. 5 and 6, where SAR values are normalized by their maxima: 100 represented by an asterisk (*), values less than 5 not presented, and tumor regions denoted by the letter *G*. These figures indicate that this APA can concentrate the EM power satisfactorily in tumor regions by properly adjusting the phase and amplitude of incident waves from the horns. For example, Fig. 5 shows that the normalized SAR in the liver tumor region is nearly 40.0 with optimized phases and amplitudes, while the SAR in most normal tissues (except the surface) is less than 20.0. By contrast, the SAR's in these regions are 35.0 and 50.0 respectively when each horn is excited with equal phase and amplitude. This means that the *H*-horn APA is rather effective and flexible in treating deep-seated tumors such as those in the liver and lungs.

If certain of the conditions discussed above are changed, we can obtain other authors' results. Satisfying (6) results in the cases of apertures and waveguides [3], [4]; changing the positions (R_i, θ_i) of the horn antennas in Fig. 1 results in the case of limited APA [5] (corresponding to the complete APA). But here the positions of sources are selected to be $R_i = 20$ cm, $\theta_i = (i-1) * 60°$, $i = 1, \cdots, 6$, while the other cases are not presented. Therefore, the formulas and methods of this paper can be applied to other types of APA systems, e.g., the aperture APA, the waveguide APA, the limited APA, and the multilayer APA.

Power absorption is primarily dictated by the conductivity or the loss factor (eq. (14)) since the *E*-field distribution does not vary a great deal within the structure. In this paper, the patient is surrounded by distilled water, shown in Fig. 3 or Fig. 4, consisting of a circular cylindrical structure, similar to Fig. 2 in geometry. The main tissues are muscle or musclelike media; i.e., the permittivities do not vary a great deal across the structures. Hence, similar *E*-field distributions but with different SAR's in the three models of Figs. 2, 3, and 4 are reasonable.

Similar observations have been made by Sathiaseelan *et al.* [4] and Paulsen *et al.* [13], who found that the *E* fields for three different body cross sections showed striking similarities despite their many anatomical differences,

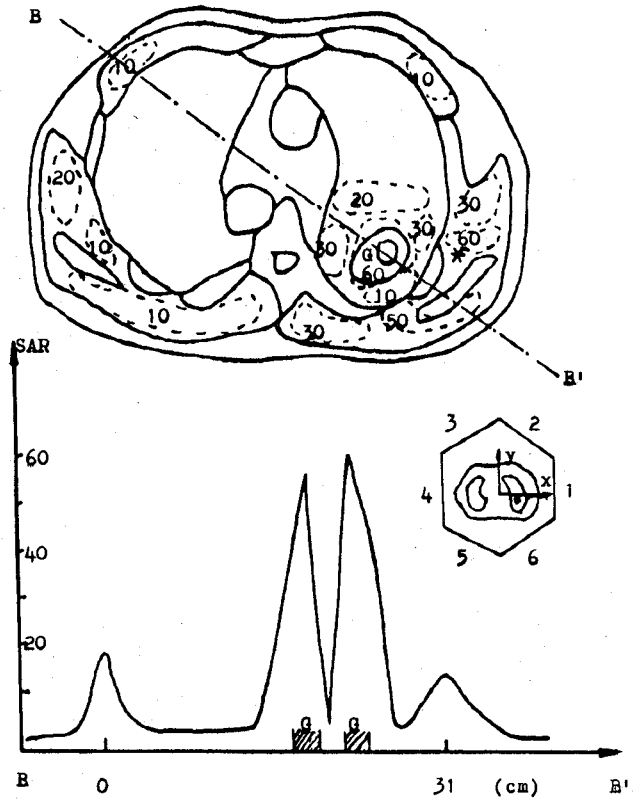

Fig. 6. The optimized SAR contours and distributions along BB' of the lung model; 180° phase lag on antennas 2,3,4,5, and 25%,15%, 15%,25% amplitude reductions on antennas 2,3,4,5.

but different electrical conductivities resulted in different absorbed powers.

V. Conclusions

The H-horn APA system is expected to be effective and attractive because of its ability to focus the power deposition in the desired regions and to move the heated regions electrically, especially in treating deep-seated tumors such as those in the liver and lungs. The numerical results indicate that a frequency of 200 MHz is appropriate for treating deep and eccentric tumors. This system has shown great promise. Of course, there will be a number of difficulties to be overcome before the technique can be used clinically.

Acknowledgment

The author would like to thank Zhang Xinghua (Chengdu Military Hospital) for providing the CT scans and Bai Lingyan for preparing the manuscript.

References

[1] C. A. Perez and J. I. Meyer, "Clinical experience with localized hyperthermia and irradiation," in *Proc. 4th Int. Symp. Hyperthermia Oncology*, 1984, vol. 2, pp. 181–198.
[2] P. F. Turner, "Regional hyperthermia with an annular phased array," *IEEE Trans. Biomed. Eng.*, vol. BME-31, pp. 106–114, Jan. 1984.
[3] C. De Wagter, "Optimization of simulated two demensional temperature distributions induced by multiple electromagnetic applicators," *IEEE Trans. Microwave Theory Tech.*, vol. MTT-34, pp. 589–596, May 1986.
[4] V. Sathiaseelan, M. F. Iskander, G. C. W. Howard and N. M. Bleehen, "Theoretical analysis and clinical demonstration of the effect of power pattern control using the annular phased-array hyperthermia system," *IEEE Trans. Microwave Theory Tech.*, vol. MTT-34, pp. 514–519, May 1986.
[5] F. Jouvie, J. C. Bolomey, and G. Gaboriaud, "Discussion of capabilities of microwave phased arrays for hyperthermia treatment of neck tumors," *IEEE Trans. Microwave Theory Tech.*, vol. MTT-34, pp. 495–501, May 1986.
[6] J. W. Strohbehn, E. H. Curtis, K. K. Paulsen, X. Yuan, and D. R. Lynch, "Optimization of the absorbed power deposition for an annular phased array hyperthermia system," *Int. J. Rad. Onc. Biol. Phys.* vol. 16, pp. 589–599, 1989.
[7] G. Arcangeli, P. P. Lombardini, G. A. Lovisolo, G. Marsiglia, and M. Piattelli, "Focusing of 915 MHz electromagnetic power on deep human tissues: A mathematical model study," *IEEE Trans. Biomed. Eng.*, vol. BME-31, pp. 47–52, 1984.
[8] D. Sullivan, "Three-dimensional computer simulation in deep regional hyperthermia using the finite-difference time-domain method," *IEEE Trans. Microwave Theory Tech.*, vol. 38, pp. 204–211, 1990.
[9] T. C. Guo, W. W. Guo, and L. E. Larsen, "A local field study of a water-immersed microwave antenna array for medical imagery and therapy," *IEEE Trans. Microwave Theory Tech.*, vol. MTT-32, pp. 844–854, Aug. 1984.
[10] R. F. Harrington, *Field Computation by Moment Methods*. New York: Macmillan, 1968.
[11] J. H. Richmond, "Scattering by a dielectric cylinder of arbitrary cross section shape," *IEEE Trans. Antennas Propagat.*, vol. AP-13, pp. 334–341, May 1965.
[12] M. A. Stuchly and S. S. Stuchly, "Dielectric properties of biological substances—Tabulated," *J. Microwave Power*, vol. 15, no. 1, pp. 19–26, 1980.
[13] K. D. Paulsen, J. W. Strohbehn, and D. R. Lynch, "Theoretical thermal dosimetry produced by an annular phased-array-type system in CT-based patient model," Radiat. Res. vol. 100, pp. 536–552, 1984.

Tianquan Deng was born in Sichuan, China, on December 23, 1964. He received the B.S. degree (with high honors) in physics from Sichuan Normal University in 1986, and the M.S. degree (with excellent levels) in microwave electronics from the University of Electronic Science and Technology of China (UESTC) in 1988.

He is presently with the Research Institute of High Energy and Microwave Electronics, UESTC. His research interests are in the areas of electromagnetic wave interactions with biological bodies, APA hyperthermia, sources of high power microwaves, free electron lasers, computer simulations, and applications to biomedical engineering.